The rotational and tunneling spectrum of the H2SCO2 van der Waals complex

Jane K. Rice, L. H. Coudert, K. Matsumura, R. D. Suenram, F. J. Lovas, W. Stahl, D. J. Pauley, and S. G. Kukolich

Citation: The Journal of Chemical Physics **92**, 6408 (1990); doi: 10.1063/1.458320
View online: http://dx.doi.org/10.1063/1.458320
View Table of Contents: http://scitation.aip.org/content/aip/journal/jcp/92/11?ver=pdfcov
Published by the AIP Publishing

The rotational and tunneling spectrum of the $H_2S \cdot CO_2$ van der Waals complex

Jane K. Rice
Code 6111, Naval Research Laboratory, Washington, DC 20375-5000

L. H. Coudert,[a] K. Matsumura,[b] R. D. Suenram, and F. J. Lovas
Molecular Physics Division, National Institute of Standards and Technology, Gaithersburg, Maryland 20899

W. Stahl
Institute of Physical Chemistry, University of Kiel, 2300 Kiel 1, Federal Republic of Germany

D. J. Pauley and S. G. Kukolich
University of Arizona, Tucson, Arizona 85721

(Received 4 December 1989; accepted 20 February 1990)

The rotational spectra of $H_2S \cdot CO_2$ and two deuterated forms have been observed using a pulsed-beam Fourier-transform microwave spectrometer. For each of the three complexes we assign *a*-type and *c*-type transitions which are split into a "weak" and a "strong" intensity component. The analysis based on that previously used for the $(H_2O)_2$ complex and modified for application to $H_2S \cdot CO_2$, allowed us to assign internal rotation, inversion tunneling states of the H_2S and CO_2 units in the complex. The following rotational constants were determined for the ground tunneling state of each species: for $H_2S \cdot CO_2$, $A = 11\,048.0(26)$ MHz, $B = 2147.786(4)$ MHz, and $C = 1806.468(4)$ MHz; for $HDS \cdot CO_2$, $A = 10\,769(35)$ MHz, $B = 2107.26(24)$ MHz, and $C = 1775.83(24)$ MHz; and for $D_2S \cdot CO_2$, $A = 10\,356.2(28)$ MHz, $B = 2065.376(8)$ MHz, and $C = 1746.122(8)$ MHz. The electric dipole moments were determined for the $H_2S \cdot CO_2$ and $D_2S \cdot CO_2$ species, resulting in the values $\mu_a = 0.410(14)$ D and $\mu_c = 0.822(10)$ D for the $H_2S \cdot CO_2$ species. The structure of the complex has the CO_2 and the S atom of H_2S in a T-shaped configuration. The H_2S plane is nearly orthogonal to the CO_2–S plane with an angle of about 92° and the $H_2S \cdot CO_2$ center-of-mass separation $R_{c.m.}$ is 3.498(3) Å.

I. INTRODUCTION

Wittig and co-workers have shown that the effects of orientation,[1] three body interactions,[2] and multiple reaction channels[3,4] can be examined by exciting a covalently bonded molecule within a van der Waals (vdW) complex such as HBr in the $HBr \cdot CO_2$ complex and examining the reaction of the translationally excited (hot) hydrogen atom with the other component of the complex. One example of this method is the following hot hydrogen atom collision with CO_2:

$$BrH \cdots CO_2 \xrightarrow{h\nu = 193\ \text{nm}} Br \cdots H \cdots CO_2 \rightarrow Br + OH + CO. \quad (1)$$

A characterization of the potential energy surface for this reaction occurring under precursor limited geometry conditions is obtained by measuring the energy disposal in the products, specifically, the internal energy of the OH fragment. Scherer *et al.*[5] have obtained information about the potential energy surface for the same reaction by measuring the appearance rate of product OH using the vdW precursor, $HI \cdot CO_2$. The effective probing of potential surfaces and the gain of dynamical information rests on the variety of hydrogen bonded complexes studied.

In some cases the information from a dynamical experiment can raise important questions about the structure of the van der Waals precursor. The internal energy content in the OH fragment formed from the hot hydrogen atom collision with CO_2 is different for the $H_2S \cdot CO_2$ and $HBr \cdot CO_2$ precursors used.[2] Although the translational energy of the hydrogen atom in the reactions is similar, the OH resulting from $H_2S \cdot CO_2$ is rotationally and vibrationally colder than that from $HBr \cdot CO_2$. This cannot be easily explained if the hydrogen atoms are experiencing the same part of the potential energy surface, i.e., if the initial impact parameters limited by the equilibrium structure are the same. One possible explanation is that the equilibrium structures of the $H_2S \cdot CO_2$ and $HBr \cdot CO_2$ complexes are different. Incorporated into this argument are differences expected from three-body interactions involving the hydrogen atom trapped between the HBr or H_2S repulsive dissociation potential and the entrance-channel barriers associated with each of the vdW precursor reactions.[6,7] If the OH due to the hydrogen atom collision originates from the precursor $H_2S \cdot CO_2$ only, this suggests a structure in which the hydrogen (including wide amplitude motion) has access to the oxygen atoms in the CO_2 species and one which is significantly different than that of $HBr \cdot CO_2$. It has been assumed for most of the work of Wittig and coworkers that the $HBr \cdot CO_2$ equilibrium structure is hydrogen bonded and linear or slightly bent

[a] National Institute of Standards and Technology Guest Worker, 1987–89 Permanent address: Laboratoire de Physique Moléculaire et Atmosphérique, Université Pierre et Marie Curie et CNRS, Tour 13, 4 Palace Jussieu, 75272 Paris Cedex 05, France.

[b] National Institute of Standards and Technology Guest Worker, 1988–89 Permanent address: Seinan Gakuin University, Nishijin, Sawaraku, Fukuoka 814, Japan.

 0021-9606/90/116408-12$03.00

based on the structures of $CO_2 \cdot HF$[8,9] and $CO_2 \cdot HCl$.[10] However, recent IR diode laser absorption measurements on $HBr \cdot CO_2$ indicate that the observed form has a T-shaped structure with the Br atom adjacent to the carbon atom of CO_2, but the location of the hydrogen atom remains poorly defined.[11]

One of the limitations in interpreting the bimolecular reaction dynamics described above is the lack of an experimentally determined structure for the $H_2S \cdot CO_2$ complex precursor. The major question is whether the lowest energy form of $H_2S \cdot CO_2$ is van der Waals bonded, hydrogen bonded or a combination of both. This was the motivation for the present structural study of $H_2S \cdot CO_2$. We present here the rotational spectra and structures for $H_2S \cdot CO_2$, $HDS \cdot CO_2$ and $D_2S \cdot CO_2$. Similar van der Waals species for which the structures have been determined are $H_2O \cdot CO_2$ and $H_2S \cdot SO_2$. The $H_2O \cdot CO_2$ complex has a T-shaped, planar structure with the hydrogens pointing away from the CO_2.[12] The $H_2S \cdot CO_2$ structure[13,14] is one in which the SO_2 and H_2S are stacked with the sulfur atoms bonded and with the hydrogen atoms pointing slightly toward the oxygen atoms. Sulfur atoms in H_2S and other sulfur containing molecules are known to include the out-of-plane lone-pair orbital in the weak bond. The structure determined for $H_2S \cdot CO_2$ is consistent with those determined for $H_2S \cdot SO_2$ and $H_2O \cdot CO_2$. In addition we present evidence of two tunneling motions in the complex.

II. EXPERIMENTAL

Fabry–Perot-cavity Fourier transform microwave spectrometers with pulsed nozzle sources were used to generate the rotational spectra of $H_2S \cdot CO_2$ and its two deuterated isotopes. The apparatus at NIST and the University of Arizona have been described in detail previously,[15,16] therefore, only modifications and experimental conditions are included here.

The supersonic expansion was created using a solenoid driven pulsed valve with a backing pressure of 0.7 to 1.2 atmospheres behind an orifice of 0.5 mm with gas pulses of 200 to 400 μs duration. The gas mixtures used contained 1% H_2S and 3% CO_2 in Ar. Three different mixtures of gases were used to identify the spectroscopic features due to $(H_2S)_2$,[17] $H_2S \cdot Ar$,[18] and $CO_2 \cdot Ar$[19]; two of these mixtures contained only one of the molecular components and the Ar carrier gas. All spectroscopic features reported here required both H_2S and CO_2 in the expansion, but not Ar as determined by substitution of Ne for Ar as the carrier gas.

Three isotopic forms are presented here, the $H_2S \cdot CO_2$ species, the monodeuterated form, $HDS \cdot CO_2$, and the dideuterated form, $D_2S \cdot CO_2$. The two deuterated forms were studied using a sample mixture containing 99% D_2S. During the early experiments with the D_2S sample, exposure to the inlet line provided enough hydrogen for exchange to occur, thus allowing the observation of the $HDS \cdot CO_2$ complex. The rotational transitions of the monodeuterated form could easily be distinguished from the dideuterated form by examining the enhancement or degradation of the spectroscopic features under study with the addition of H_2S into the nozzle inlet line. After thorough passivation with D_2S, the $D_2S \cdot CO_2$ transitions were significantly stronger than the $HDS \cdot CO_2$ transitions.

The free-induction decay signal from the cavity was digitized into 512 channels at 0.5 μs per channel. A background digitization was also done before each nozzle pulse and was subtracted from the data obtained with the nozzle on to eliminate any spurious signals produced by transmission line or cavity imperfections. Five hundred to two thousand pulses were averaged to obtain signal-to-noise ratios of about 100 to 1. The cavity bandwidth typically was on the order of 1 MHz. In order to improve the signal-to-noise response of the spectrometer, the spectra were filtered into 500 kHz windows by the preamplifier before the digitization process. The time domain signals were Fourier transformed with a frequency resolution element of 3.9063 kHz/pt. The observed spectral linewidths were typically 10^{-6} of the transition frequency (e.g., 10 kHz at 10 GHz) due to Doppler broadening.

III. RESULTS AND ANALYSIS

A. Spectral assignments

The initial frequency regions searched were based on predicted structures which placed the sulfur atom of H_2S adjacent to the C atom and perpendicular to the CO_2 axis at a distance of 3.4 Å in a fashion analogous to the planar $H_2O \cdot CO_2$ complex,[12] which has C_{2v} symmetry and an *a*-type spectrum. Since all of the previously studied complexes containing H_2S show van der Waals bonding perpendicular to the H_2S plane, a planar structure was not expected for $H_2S \cdot CO_2$. Thus, the C_2 axis of H_2S was oriented either perpendicular to the plane formed by the OCO–S atoms, which provided *a*- and *c*-type spectra, or parallel to the OCO axis, which gave *a*- and *b*-type spectra. Variation of C–S distance by ± 0.1 Å accounted for the range in predicted transitions from 11 to 13 GHz for the $J = 3$–2 *a*-type *R*-branch transitions ($\nu = 3B + 3C$) and 1_{10}–0_{00} *c*-type transition ($\nu = A + B$), while the location of the hydrogen atoms had a minor effect on the rotational constants. After searching a considerable portion of this spectral range, several pairs of lines were observed with relative intensities of approximately 3:1, which suggested a proton exchange motion in the complex. Initially only *a*-type transitions were observed (see Table I) and assignments were aided by Stark effect measurements on both states of the complex. Even after fitting the *a*-type transitions in Table I we were unable to observe the *b*- or *c*-type $J = 1$–0 transitions predicted within the frequency range searched. The fact that two complete sets of asymmetric rotor spectra were observed eliminated the planar C_{2v} structure from consideration since proton exchange in the H_2S would give two symmetry states, one with nuclear spin weight equal zero for the K_a = odd and spin weight of zero for K_a = even for the second state. Thus, a second dipole moment component had to exist.

The moderate splitting in the assigned *a*-type transitions and the observed relative intensities for the two states indicated the tunneling motion causes an exchange of the hydrogen atoms between equivalent structures, but does not invert the μ_a dipole component. The inability to detect *b*- and *c*-type transitions within ± 2 GHz of the predictions indicat-

TABLE I. Rotational spectrum of H_2S–CO_2 (MHz).

Transition	A_1 state ν^a	$\Delta\nu$	Transition	A_2 state ν^a	$\Delta\nu$
a type					
2_{12}–1_{11}				7 568.640	0.06
2_{02}–1_{01}	7 900.009	−0.03		7 905.478	0.05
2_{11}–1_{10}	8 249.376	0.00		8 242.540	0.03
3_{13}–2_{12}	11 348.914	−0.01		11 346.537	0.08
3_{03}–2_{02}	11 825.598	−0.05		11 835.504	0.07
3_{22}–2_{21}	11 853.469	0.01		11 849.884	−0.08
3_{21}–2_{20}	11 893.745	0.00		11 887.921	−0.08
3_{12}–2_{11}	12 366.886	−0.01		12 355.379	0.04
4_{14}–3_{13}	15 122.613	−0.02		15 116.967	0.06
4_{04}–3_{03}	15 722.145	−0.10		15 739.605	0.06
4_{23}–3_{22}	15 793.788	0.02		15 791.428	−0.06
4_{22}–3_{21}	15 894.644	−0.02		15 886.174	−0.06
4_{13}–3_{12}	16 475.752	−0.04		16 456.827	0.05
5_{15}–4_{14}	18 891.378	−0.03		18 877.835	0.02
5_{05}–4_{04}	19 581.048	−0.06		19 613.129	0.04
5_{24}–4_{23}	19 722.325	0.02		19 725.779	−0.02
5_{23}–4_{22}	19 925.306	−0.03		19 913.843	0.01
5_{14}–4_{13}	20 572.892	−0.07		20 539.621	0.06
6_{16}–5_{15}	22 663.679	0.05		22 627.352	−0.07
6_{06}–5_{05}	23 395.021	−0.08		23 461.545	−0.04
6_{25}–5_{24}	23 627.065	−0.08		23 651.291	0.16
6_{24}–5_{23}	23 990.694	−0.05		23 975.963	0.13
6_{15}–5_{14}	24 654.913	−0.12		24 587.600	0.06
c type					
4_{22}–3_{12}	9 159.162	−0.04	1_{01}–1_{11}	7 817.304	−0.04
4_{23}–3_{13}	11 045.928	0.00	2_{02}–2_{12}	8 154.142	−0.05
5_{23}–4_{13}	12 608.716	−0.03	3_{03}–3_{13}	8 643.106	−0.06
5_{24}–4_{14}	15 645.634	0.03	4_{04}–4_{14}	9 265.748	−0.06
6_{24}–5_{14}	16 026.514	−0.02	4_{13}–3_{03}	9 833.720	0.02
3_{13}–2_{21}	16 601.333	0.02	5_{05}–5_{15}	10 001.044	−0.04
7_{16}–8_{08}	17 170.771	0.00	6_{06}–6_{16}	10 835.239	−0.01
3_{12}–3_{20}	18 629.224	0.01	7_{07}–7_{17}	11 804.850	0.02
6_{15}–7_{07}	19 326.897	0.00	6_{24}–7_{16}	12 907.520	0.02
7_{25}–6_{15}	19 464.691	0.02	5_{14}–4_{04}	14 633.737	0.01
4_{14}–3_{22}	19 870.475	−0.01	2_{02}–1_{10}	15 385.521	0.03
6_{25}–5_{15}	20 381.331	−0.01	5_{23}–6_{15}	17 474.990	−0.06
5_{14}–6_{06}	21 831.616	0.01	7_{26}–8_{18}	18 891.377	−0.14
5_{15}–4_{23}	22 968.066	−0.05	3_{03}–2_{11}	18 978.485	0.07
4_{13}–3_{21}	23 211.240	−0.01	6_{25}–7_{17}	21 413.571	0.24
4_{13}–5_{05}	24 653.744	0.00	4_{22}–5_{14}	22 148.755	−0.01
			4_{04}–3_{12}	22 362.706	0.09
			5_{24}–6_{16}	24 126.509	−0.03
			5_{05}–4_{13}	25 519.013	0.08

[a] Estimated measurement uncertainty is 4 kHz.

ed that a second tunneling motion, which inverts the *b* or *c* dipole moment component, must be present.

Because the deuterated forms of this complex were expected to have smaller tunneling frequencies due to a larger mass, the assignment of $HDS{\cdot}CO_2$ and $D_2S{\cdot}CO_2$ was undertaken in order to resolve the question of the occurrence of a second tunneling motion. The *a*-type transitions listed in Tables II and III were readily observed and assigned via Stark effect measurements. For both deuterated species two lines were observed for each rotational transition with relative intensities of about 2:1. As anticipated, the splittings in the doublet lines for $D_2S{\cdot}CO_2$ were about a factor of 10 smaller than the corresponding splittings for $H_2S{\cdot}CO_2$, while for $HDS{\cdot}CO_2$ the splittings were intermediate between those for the H_2S and D_2S isotopic forms. Fairly extensive searches for the *b*- or *c*-type spectrum yielded two sets of *c*-type transitions offset + 2934 and − 1750 MHz from the rigid rotor predictions based on the fits of the *a*-type transitions. Since the magnitude and asymmetry in the splittings were similar to those observed for $(D_2O)_2$,[20,21] a tunneling model analogous to the water dimer model[22,23] was developed for fitting the observed spectra and is discussed in the next section.

The large tunneling shifts observed for $D_2S{\cdot}CO_2$ clearly pointed to splittings for the $H_2S{\cdot}CO_2$ species which would be five to ten times larger. During the course of this study it became known that parallel and complimentary work was in progress at both NIST and the University of Arizona. An exchange of data in a collaborative effort provided a number of *c*-type transitions for which trial assignments based on

TABLE II. Rotational spectrum of HDS–CO_2 (MHz).

Transition	Lower level[a] ν[b]	$\Delta\nu$	Transition	Upper level[a] ν[b]	$\Delta\nu$
a type					
3_{13}–2_{12}	11 142.100	−0.07		11 143.994	0.39
3_{03}–2_{02}	11 609.983	−0.08		11 599.367	0.02
3_{12}–2_{11}	12 131.290	−0.07		12 145.071	0.03
4_{14}–3_{13}	14 844.971	−0.20		14 847.255	0.29
4_{04}–3_{03}	15 435.791	−0.13		15 426.708	0.04
4_{13}–3_{12}	16 162.387	−0.02		16 175.918	−0.02
5_{15}–4_{14}	18 538.885	−0.28		18 541.234	0.02
5_{05}–4_{04}	19 224.797	−0.09		19 217.421	−0.02
5_{14}–4_{13}	20 182.119	0.08		20 195.275	−0.02
6_{16}–5_{15}	22 222.940	0.50		22 224.235	−0.43
6_{06}–5_{05}	22 970.052	0.19		22 964.129	−0.06
c type					
2_{11}–3_{03}	9 014.711	0.02			
1_{10}–2_{02}	12 532.713	−0.01	2_{11}–1_{01}	9 553.795	−0.04
6_{16}–6_{06}	17 143.158	0.11	3_{03}–2_{11}	9 790.767	0.00
5_{15}–5_{05}	17 890.258	−0.21	4_{04}–3_{12}	13 072.399	0.01
4_{14}–4_{04}	18 576.170	−0.02	3_{12}–2_{02}	13 953.676	0.06
3_{13}–3_{03}	19 166.991	0.06	5_{05}–4_{13}	16 113.905	0.01
2_{12}–2_{02}	19 634.872	0.05	4_{13}–3_{03}	18 530.223	0.01
1_{11}–1_{01}	19 958.595	0.02	6_{06}–5_{14}	18 882.759	−0.02
1_{10}–0_{00}	24 171.308	−0.03	5_{14}–4_{04}	23 298.800	−0.04

[a] This is the tunneling state within which *a*-type transitions occur. For *c*-type transitions this is the state to which the level characterized by $K_a = 0$ belongs.
[b] Estimated measurement uncertainty is 4 kHz.

TABLE III. Rotational spectrum of D_2S–CO_2 (MHz).

Transition	A_1 state ν[a]	$\Delta\nu$	Transition	A_2 state ν[a]	$\Delta\nu$
a type					
2_{11}–1_{10}	7 940.472	0.02		7 942.741	0.01
3_{13}–2_{12}	10 948.067	0.03		10 948.644	−0.01
3_{03}–2_{02}	11 398.125	−0.01		11 396.167	0.03
3_{22}–2_{21}	11 431.305	−0.03		11 429.431	−0.04
3_{21}–2_{20}	11 467.459	−0.04		11 465.423	−0.04
3_{12}–2_{11}	11 904.371	0.03		11 907.704	0.04
4_{14}–3_{13}	14 586.474	0.02		14 587.211	−0.01
4_{04}–3_{03}	15 154.723	−0.01		15 152.388	0.00
4_{23}–3_{22}	15 233.855	0.01		15 231.375	−0.02
4_{22}–3_{21}	15 324.031	0.10		15 321.035	0.01
4_{13}–3_{12}	15 860.455	0.03		15 864.455	−0.24
5_{15}–4_{14}	18 215.989	0.02		18 216.835	−0.03
5_{05}–4_{04}	18 875.712	0.02		18 873.194	−0.02
5_{24}–4_{23}	19 029.589	0.03			
5_{23}–4_{22}	19 208.367	−0.02			
5_{14}–4_{13}	19 805.748	0.01		19 810.913	0.06
6_{16}–5_{15}	21 834.952	0.02		21 835.867	−0.04
6_{06}–5_{05}	22 554.379	0.07		22 551.871	−0.05
6_{15}–5_{14}	23 736.949	−0.04		23 742.896	0.03
c type					
3_{13}–3_{03}	10 465.700	0.00	1_{10}–0_{00}	10 675.417	0.00
2_{12}–2_{02}	10 915.809	0.01	2_{11}–1_{01}	14 807.209	−0.01
1_{11}–1_{01}	11 227.250	−0.02	3_{12}–2_{02}	19 102.202	−0.01
1_{10}–0_{00}	15 357.868	−0.02	4_{13}–3_{03}	23 570.791	0.02
2_{11}–1_{01}	19 486.650	0.00			
3_{12}–2_{02}	23 776.882	0.03			

[a] Estimated measurement uncertainty is 4 kHz.

Stark effect analysis and estimated tunneling splittings led to a definitive assignment as shown in Table I for the H_2S species.

B. Dipole moment analysis

Stark effect shifts were measured for a number of transitions for the H_2S and D_2S isotopic species. A detailed description of the experimental configuration has been reported previously by Coudert *et al.*[21] Two Stark plates are located at the edge of the Fabry-Perot cavity and they are spaced by approximately 26 cm. One plate is energized with a positive voltage and the other with an equal negative voltage. This makes the electric field symmetric with respect to ground as well as allowing the application of twice the electric field obtainable from a nonsymmetric arrangement (e.g., + DC and ground). The frequency shifts of the various $|M_J|$ components are measured as a function of the applied electric field and the effective plate spacing is calibrated with measurements of the Stark effect of the $J = 1$–0 transition of OCS in the normal manner. For $H_2S \cdot CO_2$, $|M_J|$ components from five rotational transitions were measured at applied voltages up to 10 kV and least-squares fit with second order Stark coefficients generated from the Hamiltonian used for spectral fitting. The μ_a and μ_c values obtained are listed in Table IV. For $D_2S \cdot CO_2$ three transitions were measured and a total of 17 data points were fit to obtain the values listed in Table IV. It should be noted that the total dipole moments for the two isotopic forms μ_T agree within their quoted uncertainties (two standard deviations) and are nearly equal to the dipole moment of the H_2S monomer. Thus, there do not appear to be significant induced moments or large isotopic structural differences.

TABLE IV. Dipole moment components of $H_2S \cdot CO_2$ and $D_2S \cdot CO_2$.

Parameter	$H_2S \cdot CO_2$	$D_2S \cdot CO_2$
μ_a (D)	0.410(14)[a]	0.414(30)
μ_c (D)	0.822(10)	0.874(6)
μ_T (D)[b]	0.919(11)	0.965(14)

[a] One standard deviation uncertainties are given in parentheses and refer to the last digit(s) shown.
[b] μ_b (H_2S) = 0.9783 D and μ_b (D_2S) = 0.977 D from Ref. 26.

IV. ENERGY LEVELS AND ANALYSIS

In this section we seek to formulate the energy level description for $H_2S \cdot CO_2$ and $D_2S \cdot CO_2$. In these two species, because of the weakness of the hydrogen bond, many tunneling motions, such as an inversion-like wagging of the H_2S (or D_2S) subunit or a 180° rotation of the same subunit about its *b* axis, seem feasible. Based on the two different tunneling splittings observed for the *a*- and *c*-type spectra, we concluded that we are dealing with *multidimensional tunneling*, and care should be taken in order to obtain the Hamiltonian for the energy level calculation. In this paper we calculate the rovibrational energy levels using an IAM-like formalism[22,23] developed for multidimensional tunneling. This formalism is fairly straightforward to use since it does not require a detailed knowledge of the potential energy surface of the molecule being considered. However, this formalism can only be applied in the case of high barrier tunneling. For $D_2S \cdot CO_2$ and especially for $H_2S \cdot CO_2$, it is not certain yet whether this assumption is valid because of the still limited body of data available for these two species.

A. Equilibrium frameworks and tunneling paths

The determination of the molecular frameworks[22] is the first step necessary to solve the multidimensional tunneling problem. Based on the general structure for $H_2S \cdot CO_2$, described in Sec. V, there are four molecular frameworks, and they are shown in Fig. 1, where they are identified with the numbers 1, 2, 3, and 4. These frameworks were drawn with the hydrogen atoms pointing away from the CO_2 unit, which is the equilibrium configuration we favor from the results obtained in this paper. Even though only $H_2S \cdot CO_2$ is mentioned in this paragraph, everything said about this species is also assumed to be valid for $D_2S \cdot CO_2$. In Fig. 1 the *a* axis of the equilibrium configurations is almost perpendicular to the plane of the figure and approximately joins the carbon and sulfur atoms; the *x*, *y*, and *z* axes are such that the *z* axis is parallel to the *a* axis, and the *ac*-symmetry plane of the dimer is the *zx* plane. The permutation operation to be applied on

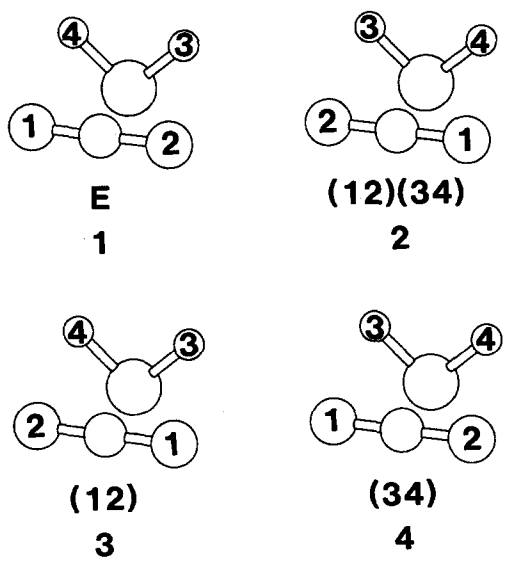

FIG. 1. The four nonsuperimposable frameworks of $H_2S \cdot CO_2$. The present figure gives a view along the molecule-fixed *z* axis, parallel to the *a* axis of the molecule. The numbers from 1 to 4, written under the frameworks, identify the equilibrium configurations. The circled numbers 1 and 2 indicate the two oxygen atoms of the CO_2 subunit, while the circled numbers 3 and 4 indicate the two hydrogen atoms of the H_2S subunits. Only strong chemical bonds within each subunit are drawn in this picture, the hydrogen bond between the CO_2 and SH_2 subunits is not represented for clarity. The permutation-inversion operation to be applied on the reference function of framework 1 in order to obtain the reference function of any framework is written under that framework. The molecule-fixed *xyz* axes are oriented for all four frameworks with the *z* axis roughly in the C–S direction, the *zx* plane is the symmetry plane, and the *y* axis is parallel to the CO_2 unit.

the reference function of framework 1 in order to obtain the wave function of a given framework is written under that framework in Fig. 1. It is worthwhile mentioning the analogy between Fig. 1 of this paper and the upper half or Fig. 3 of Hougen.[22] The molecular frameworks of Fig. 1 can be obtained from Fig. 3 by replacing the donor monomer H_1OH_2 with the carbon dioxide molecule O_1CO_2, and rotating this molecule so that O_1O_2 direction is parallel to the y axis. This analogy between $H_2S{\cdot}CO_2$ and the water dimer will be used throughout this section.

We now investigate the tunneling possibilities in $H_2S{\cdot}CO_2$. Chemical intuition suggests that three tunneling paths corresponding to rotations of the H_2S subunit about its a axis (parallel to the y axis of Fig. 1), about its b axis, or about the z axis should be feasible. More precisely, the first of these paths is an inversion-like wagging of the H_2S subunit, during which the two hydrogen atoms cross the yz plane. It will be assumed that the intermediate configuration for this tunneling path is planar with C_{2v} symmetry, the hydrogen atoms pointing away from the CO_2 subunits. This inversion-like tunneling motion connects frameworks 1 and 2 on the one hand and frameworks 3 and 4 on the other hand. The second tunneling motion can be viewed as a 180° rotation of the H_2S subunit about its symmetry axis. Since this subunit can be rotated clockwise or counterclockwise, there are actually two equivalent tunneling paths. The frameworks connected by this second tunneling motion are 1 and 4, and 2 and 3. The third tunneling motion involves a 180° rotation of the H_2S subunit about the z axis. Just as in the previous tunneling path two equivalent paths also arise depending upon the way the subunit is rotated. This last tunneling motion can also be pictured as a 180° rotation of the CO_2 subunit about the z axis, and that makes it clear that this last tunneling motion connects frameworks 1 and 3, and 2 and 4. To characterize these three tunneling motions, it is possible to make use of the number of the framework reached, when starting the motion from framework 1. The three motions we described are then the $1\rightarrow2$, $1\rightarrow4$ and $1\rightarrow3$.

As a result of the analogy between $H_2S{\cdot}CO_2$ and the water dimer, the symmetry group to be used in the present investigation is the same as the one for $H_2O{\cdot}DOD$ and will be referred in this section as G_8. The character table of this group is given in Table VIII of Coudert and Hougen.[23] The labeling of the atoms to be used in order to determine the effects of the permutation-inversion operations of this table, is given in Fig. 1.

B. Energy level diagram

The next step when using the IAM-like formalism[22,23] is the calculation of the Eulerian angles χ_n, θ_n, and ϕ_n which, through a $D^{(J)}(\chi_n,\theta_n,\phi_n)_{K'',K'}$, determine the J and K dependence of the tunneling matrix element corresponding to the $1\rightarrow n$ tunneling motion: $H_{JK'1;JK''n}$. This matrix element is calculated using the rotational wave functions defined in Eq. (24) of Hougen,[22] which are characterized by J, K, and their symmetry species in the C_s point group of the equilibrium configurations. With the I^1 representation used in this paper, the above wave functions, when they belong to the symmetry species A' (or A'') and when J is odd, correspond to the rotational levels J, $K_a=K$, $K_c=J-K+1$ (or J, $K_a=K, K_c=J-K$). When J is even the signs $'$ and $''$ must be exchanged in the previous sentence. Just as in Coudert and Hougen,[23] symmetry relations arise for the Eulerian angles χ_n, θ_n, and ϕ_n so that only two parameters and sometimes only one are needed to characterize the J and K dependence of the tunneling matrix element. The derivation of these symmetry relations will not be explained in this paper.

Let us first consider the $1\rightarrow2$ tunneling motion. A careful examination of this tunneling motion shows that this motion has the same symmetry properties as the one also called "$1\rightarrow2$" in the water dimer.[23] We therefore have $\chi_2=0$ and $\phi_2=\pi$, while θ_2 can have any value, and the diagonal tunneling matrix element, $H_{JK1;JK2}$, can be obtained using Eqs. (33) and (34) of Coudert and Hougen[23]:

$$\begin{aligned}
H_{JK1';JK2'} &= +h_{2v}(-1)^K\left[d^{(J)}(\theta_2)_{K,K}\right.\\
&\quad\left.+(-1)^{J+K}d^{(J)}(\theta_2)_{K,-K}\right],\\
H_{JK1'';JK2''} &= +h_{2v}(-1)^K\left[d^{(J)}(\theta_2)_{K,K}\right.\\
&\quad\left.-(-1)^{J+K}d^{(J)}(\theta_2)_{K,-K}\right],\\
H_{JK1';JK2''} &= H_{JK1'';JK2'}=0,
\end{aligned}\tag{2}$$

where the primes and double primes are a shorthand notation for the rotational symmetry species A' and A''. For $K=0$ the right terms of Eqs. (2) must be divided by 2. For the two remaining tunneling motions ($1\rightarrow3$ and $1\rightarrow4$), which are both characterized by the fact that they can be performed in two different but energetically equivalent ways, examining the paths shows that symmetry relations, analogous to those given in Eqs. (17) and (24) of Coudert and Hougen[23] for the "$1\rightarrow4$" motion of the water dimer, are fulfilled. As a consequence the Eulerian angles for the $1\rightarrow3$ and $1\rightarrow4$ motion will satisfy the symmetry relations: $\chi_3=\phi_3+\pi$ and $\chi_4=\phi_4+\pi$, θ_3 and θ_4 having any value. Also Eqs. (35) and (36) of Coudert and Hougen[23] can be used to obtain expressions for the diagonal matrix elements, $H_{JK1;JK3}$ and $H_{JK1;JK4}$:

$$\begin{aligned}
H_{JK1';JK3'} &= 2h_{3v}(-1)^K\left[d^{(J)}(\theta_3)_{K,K}\cos(2K\phi_3)\right.\\
&\quad\left.+(-1)^{J+K}d^{(J)}(\theta_3)_{K,-K}\right],\\
H_{JK1'';JK3''} &= 2h_{3v}(-1)^K\left[d^{(J)}(\theta_3)_{K,K}\cos(2K\phi_3)\right.\\
&\quad\left.-(-1)^{J+K}d^{(J)}(\theta_3)_{K,-K}\right],\\
H_{JK1';JK3''} &= H_{HJ1'';JK3'}=0,
\end{aligned}\tag{3}$$

the expression of $H_{JK1;JK4}$ being obtained replacing the subscript 3 by the subscript 4. In Eqs. (3) the signs prime and double prime are defined as for Eqs. (2); a division by 2 must also be carried out for $K=0$. As emphasized by Eqs. (2) and (3), the effect of the symmetry relations on the Eulerian-type angles is to reduce the number of independent parameters involved in the J and K dependence of the tunneling splittings from 9 to 5. More precisely, the five remaining parameters are θ_2, θ_3, ϕ_3, θ_4, and ϕ_4. A numerical calculation of these angles could be performed guessing the various tunneling paths and then using Eqs. (49) of Hougen.[22] However, such a calculation will not be attempted in this paper. An estimation will be performed considering the lightness of

TABLE V. Energy level expressions for $H_2S \cdot CO_2$ and $D_2S \cdot CO_2$.

Symmetry species		
Rotation[a]	Overall[b]	Energy
A'	A_1^+	$H_{JK1';JK1'} + H_{JK1';JK2'} + H_{JK1';JK3'} + H_{JK1';JK4'}$
A'	B_1^-	$H_{JK1';JK1'} - H_{JK1';JK2'} - H_{JK1';JK3'} + H_{JK1';JK4'}$
A'	B_2^+	$H_{JK1';JK1'} + H_{JK1';JK2'} - H_{JK1';JK3'} - H_{JK1';JK4'}$
A'	A_2^-	$H_{JK1';JK1'} - H_{JK1';JK2'} + H_{JK1';JK3'} - H_{JK1';JK4'}$
A''	A_1^-	$H_{JK1'';JK1''} + H_{JK1'';JK2''} + H_{JK1'';JK3''} + H_{JK1'';JK4''}$
A''	B_1^+	$H_{JK1'';JK1''} - H_{JK1'';JK2''} - H_{JK1'';JK3''} + H_{JK1'';JK4''}$
A''	B_2^-	$H_{JK1'';JK1''} + H_{JK1'';JK2''} - H_{JK1'';JK3''} - H_{JK1'';JK4''}$
A''	A_2^+	$H_{JK1'';JK1''} - H_{JK1'';JK2''} + H_{JK1'';JK3''} - H_{JK1'';JK4''}$

[a] Symmetry species of the rotational wave function in the point group C_s.
[b] Symmetry species of the rovibrational wave function in the group G_8 of Table VIII of Coudert and Hougen (Ref. 23).

the hydrogen atoms, and the fact that the CO_2 unit has much larger moments of inertia than the H_2S unit. It can then be shown that θ_2, θ_3, and θ_4 are of the order a few degrees, that $\phi_3 \simeq \pi$ while $\phi_4 \simeq \pi/2$. Replacing these approximate values in the expressions of the tunneling matrix elements in Eqs. (2) and (3), and taking into account the fact that the term $d^{(J)}(\theta)_{K',K''}$ which appears in these equations is roughly equal to $\delta_{K',K''}$ when θ is small, gives the following approximate expressions for the tunneling matrix elements:

$$\begin{aligned} H_{JK1;JK2} &= +h_{2v}(-1)^K, \\ H_{JK1;JK3} &= +2h_{3v}(-1)^K, \\ H_{JK1;JK4} &= +2h_{4v}, \end{aligned} \tag{4}$$

which are only valid when the two rotational wave functions have the same symmetry species.

Setting up the Hamiltonian matrix is straightforward and can be done using group theory. In Table V the expression of the eigenvalues and the symmetry species of the corresponding eigenvector in the group G_8 are given. In this table $H_{JK1';JK1'}$ and $H_{JK1'';JK1''}$ are the diagonal matrix elements of a usual rotational Hamiltonian within rotational wave functions of A' and A'' symmetry species. We have

$$\begin{aligned} H_{JK1';JK1'} &= [A - \tfrac{1}{2}(B+C)]K^2 + \tfrac{1}{2}(B+C)J(J+1) \\ &\quad + \tfrac{1}{4}(-1)^J(B-C)J(J+1)\delta_{K,1} \\ H_{JK1'';JK1''} &= [A - \tfrac{1}{2}(B+C)]K^2 + \tfrac{1}{2}(B+C) \\ &\quad \times J(J+1) - \tfrac{1}{4}(-1)^J(B-C)J(J+1)\delta_{K,1}. \end{aligned} \tag{5}$$

Using Eqs. (4) and (5) and Table V, it is quite easy to draw the energy level diagram. This is done in Fig. 2, making the assumption $h_{2v} < h_{3v} < h_{4v} < 0$. As emphasized by this figure, the effects of the large amplitude motions are to split each rotational energy level into four sublevels, two of them having a zero statistical weight due to the zero nuclear spins of the oxygens of CO_2. To draw the transitions in Fig. 2, the following selection rule was used: $X^+ \leftrightarrow X^-$, where $X = A_1$, A_2, B_1, and B_2. The a-type transitions display no direct effects of the large amplitude motions because they occur within a tunneling level. The small splittings actually ob-

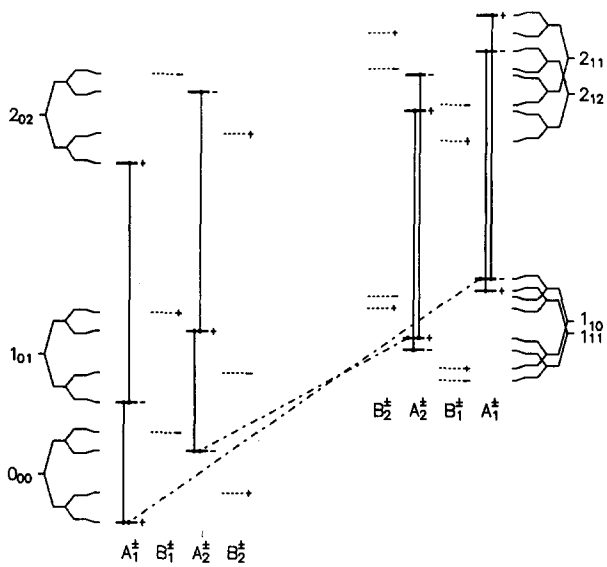

FIG. 2. Energy levels (not to scale) of $H_2S \cdot CO_2$ with $J \leq 2$ and $K_{-1} \leq 1$. Each rotational level is split into four sublevels by the large amplitude motions. The straight horizontal line near the rotational label indicates the position of the levels when no tunneling is present. Starting from this horizontal line, and going to the right we first see the effects of the $1 \rightarrow 2$ tunneling motion. This motion splits the rotational levels into two sublevels. Going further to the right, the $1 \rightarrow 3$ tunneling motion is turned on and this leads to a splitting of the two previous levels into two sublevels. Considering at last the $1 \rightarrow 4$ motion does not result in a further splitting of these sublevels, but just shifts them up or down. The levels are labeled with their symmetry species in the G_8 symmetry group. Each stack in the present figure corresponds to one of the four pair $A_1^\pm$, $A_2^\pm$, $B_1^\pm$, and $B_2^\pm$. The + or − signs appearing on the right of the rovibrational levels define completely the symmetry species. For $H_2S \cdot CO_2$ ($D_2S \cdot CO_2$) the statistical weights are 1 and 3 (2 and 1) for the symmetry species $A_1^\pm$ and $A_2^\pm$, respectively. For the other symmetry species, indicated by a horizontal dashed line in the present figure, the statistical weight is zero. Some of the a-type transitions are indicated in this picture. These transitions occur within a given tunneling level and do not display any first order effects of the tunneling. This is not true for the c-type transitions which are shifted by the tunneling. In the present picture only two c-type transitions, between $J = 0$ and $J = 1$, are drawn with alternate dashed dotted lines. When using this picture for the less symmetrical species, $HDS \cdot CO_2$, the subscripts 1 and 2 on the symmetry species labels must be dropped since only four symmetry species arise: $A^\pm$ ($g = 1$) and $B^\pm$ ($g = 0$).

served in the *a*-type spectrum indicate an indirect effect of the large amplitude motions and arise because each tunneling state is characterized by slightly different rotational constants (which was ignored in Fig. 2). Only the *c*-type transitions allow us a direct measurement of some of the tunneling splittings. Examining Fig. 2 closely, one sees that two *c*-type bands are expected but they are shifted from rigid rotor predictions by amounts equal to $+2(h_{2v}+2h_{3v})$ or to $-2(h_{2v}-2h_{3v})$. Since h_{4v} does not appear in these expressions, it is not possible to obtain a direct estimation of the tunneling splitting associated with the $1\rightarrow4$ motion, consisting of a rotation of the H_2S subunit about its C_2 axis of symmetry, using only the microwave spectrum of the dimer.

C. Analysis

In order to analyze the microwave spectrum, a computer program was written in which the energy levels were calculated using the formalism outlined in the previous paragraph. In this program the Hamiltonian submatrices corresponding to each tunneling symmetry species were diagonalized separately. The diagonal matrix elements of these submatrices were calculated using Table V and Eqs. (2), (3), and (5). The nondiagonal matrix elements, with $\Delta K>1$, arising from the rigid rotor as well as from the vibrational part of the Hamiltonian were also taken into account. The expression of these latter terms will not be given in this paper, but can be obtained from Coudert and Hougen.[24] Distortion effects were also taken into account in the analysis. For the rigid rotor part of the Hamiltonian, a Watson[25] S-reduced set of distortion constants was used, while for the vibrational part of the Hamiltonian the distortion parameters of Coudert and Hougen[23] were utilized. The parameters determined in the analysis are given in the first column of Table VI, and the values for the two symmetrical isotopic species in the second and fourth columns. In this table the parameters related to the rotational Hamiltonian are given first. Then come those related to the $1\rightarrow2$ and $1\rightarrow3$ motions. The parameters h_{nk}, h_{nj}, f_n, etc, $n=2$ or 3, are the distortion parameters introduced by Coudert and Hougen.[23] Since, as pointed out in the previous paragraph, the $1\rightarrow4$ motion does not give rise to any direct effects in the *a*-type as well as in the *c*-type spectrum, the parameters relevant to this motion are ill defined and were set equal to zero. They, therefore, do not appear in Table VI. The observed frequencies, the assignments, and the observed minus calculated differences ($\Delta\nu$) of the transitions included in the fit are reported in Table I for $H_2S{\cdot}CO_2$ and in Table III for $D_2S{\cdot}CO_2$.

The parameters related to the J and K dependence of the various tunneling splittings, more precisely the angles given in Table VI, can be used to quantitatively refine the parameterization of the tunneling paths. Let us consider the $1\rightarrow2$ motion, corresponding to the inversion-like rotation of the H_2S subunit about its *a* axis. If we assume that the inertia tensor does not change too much during the motion, it is possible to solve Eqs. (49) of Hougen,[22] and to thereby obtain the expression of the angle θ_2 as a function of the equilibrium parameters of the dimer. Let α be the angle of the C_2 axis of the H_2S subunit with the *a* axis of the dimer, the angle through which the H_2S subunit is rotated during the large amplitude motion is 2α. Solving Eqs. (49) of Hougen[22] leads to

$$\theta_2 = 2\alpha\cdot B(H_2S{\cdot}CO_2)/A(H_2S), \tag{6}$$

where $B(H_2S{\cdot}CO_2)$ is the rotational constant of the entire dimer, and $A(H_2S)$ is the rotational constant of the H_2S subunit about its *a* axis. Equation (6), also valid for

TABLE VI. Rotational and tunneling constants for $H_2S{\cdot}CO_2$, $HDS{\cdot}CO_2$, and $D_2S{\cdot}CO_2$.

Parameter		$H_2S{\cdot}CO_2$	$HDS{\cdot}CO_2$	$D_2S{\cdot}CO_2$
A	(MHz)	11 048.0(26)[a]	10 769.(35)[a]	10 356.2(28)[a]
$\frac{1}{2}(B+C)$	(MHz)	1 977.126 8(31)	1 941.57(23)	1 905.749 4(46)
$(B-C)$	(MHz)	341.318 3(48)	331.37(16)	319.254(14)
D_J	(kHz)	8.955(55)	8.58[c]	8.200(80)
D_{JK}	(MHz)	0.175 82(78)	1.15(44)	0.139 1(25)
d_1	(kHz)	1.764(41)	3.65(33)	1.244(68)
d_2	(kHz)	−0.337(32)	−0.35[c]	−0.362(95)
h_2	(MHz)	−12 521.927(46)	−4 713.55(10)	−1 170.752(13)
θ_2	(deg)	0.793 80(46)	0.761(57)	1.872(63)
h_{2k}	(MHz)	10.732(19)	0[b]	0[b]
h_{2j}	(kHz)	281.0(21)	169.(30)	−159.(22)
f_2	(kHz)	−77.49(92)	−132.(17)	57.(12)
h_{2jk}	(kHz)	−10.05(80)	0[b]	0[b]
h_{2jj}	(kHz)	0.104(50)	0[b]	0[b]
h_3	(MHz)	−2 100.8(13)	−484.(11)	−148.81(71)
ϕ_3	(deg)	180[b]	180[b]	180[b]
θ_3	(deg)	0.388 398(69)	1.73(27)	0.701(86)
h_{3k}	(MHz)	42.7(13)	32.6(93)	0[b]
h_{3j}	(MHz)	−0.166 69(85)	−0.38(13)	0[b]

[a] The standard deviation is given in parentheses and refers to the last digits shown.
[b] Constrained value.
[c] Parameter constrained to a value determined from the analysis of the two symmetrical isotopic species.

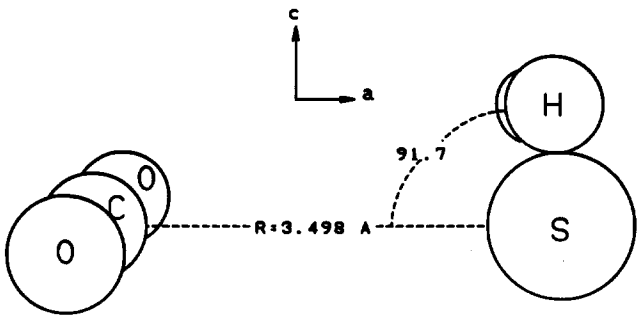

FIG. 3. Molecular structure of $H_2S{\cdot}CO_2$ based on the case C fit to $R_{c.m.}$ and $\Theta(\angle C\text{–c.m.–S}) = 87.4°$ with the Θ_1 ($\angle C$–S–c.m.) value shown. The *a* axis is nearly coincident with the line joining the C and S atoms and the *a*, *c* axes define the symmetry plane.

$D_2S{\cdot}CO_2$, leads to the following values of α: 57.4° and 74.3° for $H_2S{\cdot}CO_2$ and $D_2S{\cdot}CO_2$, respectively. The values reported in Table VI for θ_2 were used in this calculation.

D. The HDS·CO_2 dimer

The $HDS{\cdot}CO_2$ dimer cannot be treated with the completely protonated and completely deuterated species because it lacks the plane of symmetry that these two latter species possess. The symmetry group to use for this partially deuterated species is G_4, the character table of which is given in Table X of Coudert and Hougen.[23] Figure 1 can still be used to obtain the various frameworks of the dimer but the four symmetry operations used to generate the framework wavefunctions must be replaced by E, E^*, (12), and (12)*. The symmetry properties of the tunneling motions must also be reviewed. For instance the $1 \rightarrow 4$ motion no longer corresponds to two equivalent tunneling paths, but to two *inequivalent* tunneling paths. However, as a consequence of the lightness of the hydrogen and deuterium atoms, we can assume that the energy level diagram, for low J and K values, is not very different from the one given for the two symmetrical species. Figure 2 can be used once the subscripts 1 and 2 on the labels for the symmetry species of the levels are removed. To analyze the transitions, it is also possible to use the formalism described in the previous paragraph. The results of such an analysis are given in the third column of Table VI, where the parameters are reported, and in Table II where the assignment, the observed minus calculated values ($\Delta\nu$) and the observed frequency of the transitions included in the fit are given.

V. STRUCTURE ANALYSIS

Both a T-shaped and a more prolate hydrogen-bonded structure were considered, however, only the T-shaped configuration of the S–CO_2 plane is consistent with the magnitude of the rotational constants. The existence of only *a*- and *c*-dipole moment components indicates that the H_2S C_2 axis (the dipole axis) lies in the *a*, *c* plane of the complex, and the derived inertial defect, $\Delta = -1.28$ uÅ^2, indicates that the hydrogen atoms are above the plane of the heavy atoms. Using the usual assumption that the monomer geometries do not change upon complex formation, only two additional structural parameters, $R_{c.m.}$ and Θ (the C–c.m.–S angle), are required to define the structure as shown in Fig. 3. With only two variables, structural calculations can be carried out in several ways. Three types of calculations were performed with the monomer parameters fixed at the values: $r_{CO} = 1.1621$ Å, $r_{SH} = 1.3361$ Å, and $\angle$ HSH = 92.18°. For case A each isotopic species was fit individually to determine Θ and R_{cm} as shown in Table VII by fitting the I_a, I_b, and I_c moments of inertia starting with an acute angle of Θ. In case B an obtuse angle of Θ was determined, which is effectively the supplementary angle of case A. In case C of Table VII data for all three isotopic species were employed. In one set, the I_b and I_c moments were fit since the A rotational constant has the largest uncertainty and correlation with the tunneling terms. The second fit for all species employed the second moments of inertia P_{aa} and P_{bb}, where $P_{aa} = \frac{1}{2}(I_b + I_c - I_a)$ and $P_{bb} = \frac{1}{2}(I_a + I_c - I_b)$, with the results given in Table VII. The major difference in the structural parameters from these three cases is in the value of Θ. In case A, Θ ranges from 39° to 54°, and in case B, Θ ranges from 141° to 127° for the three isotopic species. For the global fit of case C, Θ is about 87° for the two methods employed. Also listed in Table VII are Θ_1 (the C–S–c.m. angle), R_{CS}, R_{OH}, and the hydrogen atom coordinates obtained for each case. In order to determine if the coordinates of any of these analyses are consistent with a substitution coordinate analysis, a Kraitchman[27] single substitution calculation was carried out with the H_2S/HDS and D_2S/HDS pairs of species, and a double substitution calculation following Chutjian[28] was performed with the H_2S/D_2S species. The resulting principal axes coordinates are given in Table VIII. The substitution coordinates, particularly a_H, agree best with the coordinates from the simultaneous fit to all species in case C, which suggests that this is the most representative structure for the complex. We are somewhat cautious about emphasizing this agreement between the Kraitchman (and Chutjian) calculations and the case C structural fits because the effect of multidimensional tunneling on these calculations is not known.

In many cases the dipole moment data is employed to obtain angular information on the structure of complexes. In the present case, if one neglects any induced moment effects, the angle between the *a*-axis of the complex and C_2 axis of H_2S is calculated to be $\Theta_1 = 116.6°$ (or $\Theta = 180° - \Theta_1 = 63.4°$) from a simple projection of the μ_b moment of H_2S. A similar result is obtained for $D_2S{\cdot}CO_2$ as shown at the bottom of Table VII. Also, as mentioned above, the angle α employed in the inversion motion analysis can be used to derive Θ_1 with the results summarized in Table VII. While these estimates are in better agreement with the results of the case A and B fits, they may be less reliable due to the assumptions made in these estimates. For example, a small μ_c (induced) of -0.1 to -0.15 D would be consistent with the plane of H_2S perpendicular to the heavy atom plane ($\Theta_1 = 90°$). There is less experience in using the angular motion from the tunneling motion for structural information. On the other hand the 92° angle for the C- -S van der

TABLE VII. Molecular structure parameters (Å).

Case A: Moments I_a, I_b, and I_c are used, fit $\Theta < 90°$ and $R_{c.m.}$	$H_2S{\cdot}CO_2$	$HDS{\cdot}CO_2$	$D_2S{\cdot}CO_2$
Θ	34.4(11)°	42.1(28)°	54.1(30)°)
$R_{c.m.}$	3.491(1)	3.471(2)	3.464(3)
σ (u Å^2)	0.04	0.14	0.19
Θ_1	140.0(11)°	137.3(28)°	125.1(30)°
$R_{C\text{-}S}$	3.449(1)	3.431(3)	3.432(4)
$R_{O\text{-}H}$	4.206(9)	4.164(24)	4.042(32)
a_H	2.64	2.61	2.48

Case B: Moments I_a, I_b, and I_c are used, fit $\Theta > 90°$ and $R_{c.m.}$	$H_2S{\cdot}CO_2$	$HDS{\cdot}CO_2$	$D_2S{\cdot}CO_2$
Θ	140.6(11)°	138.6(33)°	127.1(30)°
$R_{c.m.}$	3.491(1)	3.508(1)	3.522(2)
σ(u Å^2)	0.04	0.17	0.19
Θ_1	38.8(10)°	40.8(33)°	52.2(30)°
$R_{C\text{-}S}$	3.534(1)	3.550(3)	3.555(3)
$R_{O\text{-}H}$	2.878(13)	2.919(40)	3.081(42)
a_H	1.29	1.32	1.46

Case C: Fit three isotopic species to Θ and $R_{c.m.}$ Moments:	I_b, I_c	P_{aa}, P_{bb}
Θ	87.9° ± 5°	87.4 ± 2°
$R_{c.m.}$	3.494(3)	3.498(2)
σ (u Å^2)	0.62	0.11
Θ_1	91.2° ± 5°	91.7 ± 2°
$R_{C\text{-}S}$	3.493(6)	3.496(2)
$R_{O\text{-}H}$	3.637(78)	3.649(19)
a_H	2.003	2.013
b_H	0.963	0.963
c_H	0.870	0.870

Angle Θ_1 derived from dipole moment and tunneling angle	$H_2S{\cdot}CO_2$	$D_2S{\cdot}CO_2$
Θ_1(dipole)	116.6°/63.4°	115.1°/64.9°
Θ_1(tunneling)	122.6°/57.4°	105.7°/74.3°

Waals interaction is consistent with other complexes containing H_2S. With the same definition of Θ_1, the value for Θ_1 in $H_2S{\cdot}HCl$[29] is 86.2°, for $H_2S{\cdot}HBr$[30] $\Theta_1 = 83.5°$ and for $H_2S{\cdot}HCN$[31] $\Theta_1 = 95.4°$.

VI. DISCUSSION

Only recently have a number of similar asymmetric rotor van der Waals (vdW) complexes been analyzed. The most relevant to this study are the reports of the $H_2O{\cdot}CO_2$ complex[12] and the $H_2S{\cdot}SO_2$ complex.[13,14] The structure we present here for $H_2S{\cdot}CO_2$ is consistent with a hybrid of the $H_2O{\cdot}CO_2$ and $H_2S{\cdot}SO_2$ structures. In the $H_2S{\cdot}CO_2$ complex the tendency for the sulfur atom to bond at 90° to the plane of the monomer H_2S is similar to that seen in the $H_2S{\cdot}SO_2$ structure, while the T shape of the $S{\cdot}CO_2$ portion of the complex is exactly that seen in the $H_2O{\cdot}CO_2$ complex. Other systems which are more peripherally related are $H_2O{\cdot}SO_2$ [14] and $H_2O{\cdot}O_3$.[32] A comparison of the bonding in $H_2O{\cdot}SO_2$ and $H_2S{\cdot}SO_2$ is made in Ref. 14.

In the five vdW complexes mentioned above, we find varying types of internal motions and magnitudes of spectral splittings. The $H_2S{\cdot}CO_2$ complex has two distinct tunneling

TABLE VIII. Substitution coordinates for hydrogen (Å).

	a_H	b_H	c_H
Single substitution			
H_2S/HDS	2.024	0.867	0.677
D_2S/HDS	1.969	0.953	0.946
Double substitution			
H_2S/D_2S	2.013	0.910	0.855

TABLE IX. Comparison of vdW radii, experimental bond lengths, stretching frequencies ω_s, and force constants k_s.

	Bond	vdW Radii (Å)[a]	Experimental Distance (Å)	ω_s (cm^{-1})	k_s (mdyn/Å)
$H_2S \cdot CO_2$	C–S	3.47	3.49	55.8	0.035
$H_2O \cdot O_3$[b]	O–O	3.0	3.17[c]	70.3	0.038
$H_2S \cdot SO_2$[b]	S–S	3.6	3.520[d]	57.0	0.043
$D_2O \cdot CO_2$[b]	C–O	3.17	2.836[e]	80.2	0.052
$H_2O \cdot SO_2$[b]	S–O	3.3	2.824[b]	80.1	0.053

[a] Calculated assuming C = 1.67, S = 1.8, and O = 1.5 Å.
[b] Values of ω_s and k_s taken from Ref. 14.
[c] Reference 32.
[d] Reference 14, recalculation of Ref. 13.
[e] Reference 12.

motions, whereas, the $H_2O \cdot O_3$, $H_2O \cdot CO_2$ and $H_2O \cdot SO_2$ complexes exhibit splitting due to one tunneling motion which is thought to be an internal rotation of H_2O about its C_2 axis. The $H_2S \cdot SO_2$ spectrum exhibits no tunneling motions. The inversion motion exhibited by $H_2S \cdot CO_2$ is unique among these complexes, due in part to the fact that both subunits of the complexes with two asymmetric top subunits would have to participate in the large amplitude motion which very likely would have a much higher barrier than that for the tunneling of one subunit. This information coupled with the geometries and strength of the vdW bonds gives a more complete picture of the potential energy surface for these complexes.

Since the H–O distance in all of these complexes is large (> 3 Å), there is little or no hydrogen bonding evident. Thus, the dominant bonding forces must be attributed to electrostatic and dispersion interactions. If we examine the calculated force constants generated from the pseudodiatomic model[33] for these complexes shown in Table IX, we find that the weakest vdW bond is that of $H_2S \cdot CO_2$ which is consistent with the large tunneling terms. Also included in Table IX is the sum of the vdW radii compared with the experimental bond distance for the five species. The similarity of the added radii verses the experimental distance in $H_2S \cdot CO_2$, $H_2O \cdot O_3$, and $H_2S \cdot SO_2$ indicate vdW-type bonding. The shorter experimental distances in $D_2O \cdot CO_2$ and $H_2O \cdot SO_2$ suggest a somewhat stronger vdW bond and correlate well with the magnitude of the force constants. A direct correlation between the presence and magnitude of tunneling splittings and the weakness of the vdW bond is too simplistic an expectation since there are too many distinct geometries and types of internal motions in this series, but qualitatively the tunneling splittings for these species appear to follow a trend inversely proportional to the force constants with the largest splittings for $H_2S \cdot CO_2$ and the smallest for $H_2O \cdot CO_2$ and $H_2O \cdot SO_2$.

We have determined that in the equilibrium geometry of $H_2S \cdot CO_2$ the hydrogens of H_2S are located ~90° out of the S–CO_2 plane. This structure poses several interesting questions for the interpretation of the precursor limited geometry bimolecular reaction work with $H_2S \cdot CO_2$ as precursor.[2] Using the potential energy surface calculated by Schatz, Fitcharles, and Harding[34] for a hot H atom approaching CO_2, we conclude that the H atom must have a fairly direct approach toward the C or O atoms of CO_2 for reaction to occur. Due to the multidimensional tunneling in the complex, there is a possibility that the H atoms are located in regions between the S atom and the CO_2 unit while the dissociation of H_2S occurs. It might be noted that the higher the barriers for these tunneling motions, the smaller is the probability for the existence of this transition state geometry for the optimal reaction configuration. In summary, the apparent lack of hydrogen bonding and the occurrence of multidimensional tunneling in this complex introduces complications in the interpretation of the dynamical results observed under precursor limited geometry conditions.

The present understanding of the geometry and internal dynamics would benefit from complementary *ab initio* calculations. The support from theoretical calculations regarding the location of the H atoms is particularly important. Equally important would be a theoretical determination of the tunneling paths and barriers in this complex to help resolve questions concerning secondary bonding between the hydrogens and oxygens and the probability of finding the hydrogen atoms between the two subunits.

[1] G. Radhakrishnan, S. Buelow, and C. Wittig, J. Chem. Phys. **84**, 727 (1986).
[2] J. Rice, G. Hoffman, and C. Wittig, J. Chem. Phys. **88**, 2841 (1988).
[3] D. Häusler, J. Rice, and C. Wittig, J. Chem. Phys. **91**, 5413 (1987).
[4] G. Hoffman, D. Oh, H. Iams, and C. Wittig, Chem. Phys. Lett. **155**, 356 (1989).
[5] N. F. Scherer, L. R. Khundkar, R. B. Bernstein, and A. H. Zewail, J. Chem. Phys. **87**, 1451 (1987).
[6] C. Wittig, Y. M. Engel, and R. D. Levine, Chem. Phys. Lett. **153**, 411 (1988).
[7] C. Wittig, S. Sharpe, and R. A. Beaudet, Acc. Chem. Res. **21**, 341 (1988).
[8] F. A. Baiocchi, T. A. Dixon, C. H. Joyner, and W. Klemperer, J. Chem. Phys. **74**, 6544 (1981).
[9] C. M. Lovejoy, M. D. Schuder, and D. J. Nesbitt, J. Chem. Phys. **86**, 5337 (1987).
[10] R. S. Altman, M. D. Marshall, and W. Klemperer, J. Chem. Phys. **77**, 4344 (1982).
[11] S. Sharpe, Y. Zeng, C. Wittig, and R. Beaudet, J. Chem. Phys. **92**, 943 (1990).
[12] K. I. Peterson and W. Klemperer, J. Chem. Phys. **80**, 2439 (1984).
[13] R. E. Bumgarner, D. J. Pauley, and S. G. Kukolich, J. Chem. Phys. **87**,

3749 (1987).
[14]K. Matsumura, F. J. Lovas, and R. D. Suenram, J. Chem. Phys. **91**, 5887 (1989).
[15]R. E. Bumgarner and S. G. Kukolich, J. Chem. Phys. **86**, 1083 (1987).
[16]F. J. Lovas and R. D. Suenram, J. Chem. Phys. **87**, 2010 (1987); R. D. Suenram, F. J. Lovas, G. T. Fraser, J. Z. Gillies, C. W. Gillies, and M. Onda, J. Mol. Spectrosc. **136**, 127 (1989).
[17]F. J. Lovas, R. D. Suenram, and K. Matsumura (private communication, 1989).
[18]R. Viswanathan and T. R. Dyke, J. Chem. Phys. **82**, 1674 (1985).
[19]J. M. Steed, T. A. Dixon, and W. Klemperer, J. Chem. Phys. **70**, 4095 (1979); G. T. Fraser, A. S. Pine, and R. D. Suenram, *ibid.* **88**, 6157 (1988).
[20]J. A. Odutola, T. A. Hu, D. Prinslow, S. E. O'dell and T. R. Dyke, J. Chem. Phys. **88**, 5352 (1988).
[21]L. H. Coudert, F. J. Lovas, R. D. Suenram, and J. T. Hougen, J. Chem. Phys. **87**, 6290 (1987); R. D. Suenram, G. T. Fraser, and F. J. Lovas, J. Mol. Spectrosc. **138**, 440 (1989).
[22]J. T. Hougen, J. Mol. Spectrosc. **114**, 395 (1985).
[23]L. H. Coudert and J. T. Hougen, J. Mol. Spectrosc. **130**, 86 (1988).
[24]L. H. Coudert and J. T. Hougen, J. Mol. Spectrosc. **139**, 259 (1990).
[25]J. K. G. Watson, in *Vibrational Spectra and Structure*, edited by J. R. Durig (Elsevier, Amsterdam, 1977), Vol. 6, p. 1.
[26]R. Viswanathan and T. R. Dyke, J. Mol. Spectrosc. **103**, 231 (1984).
[27]J. K. Kraitchman, Amer. J. Phys. **21**, 17 (1953).
[28]A. Chutjian, J. Mol. Spectrosc. **14**, 361 (1964).
[29]E. J. Goodwin and A. C. Legon, J. Chem. Soc. Faraday Trans. 2 **80**, 51 (1984).
[30]A. I. Jaman and A. C. Legon, J. Mol. Struct. **145**, 261 (1986).
[31]E. J. Goodwin and A. C. Legon, J. Chem. Soc., Faraday Trans. 2, **80**, 1669 (1984).
[32]J. Z. Gillies, C. W. Gillies, R. D. Suenram, F. J. Lovas, T. Schmidt, and D. Cremer, J. Chem. Phys. (submitted).
[33]D. J. Millen, Can. J. Chem. **63**, 1477 (1985).
[34]G. C. Schatz, M. S. Fitcharles, and L. B. Harding, Faraday Discuss. Chem. Soc. **84**, 359 (1987).